Soft Matter

PAPER

View Article Online
View Journal | View Issue

Cite this: *Soft Matter*, 2014, **10**, 5916

Insights into ordered microstructures and ordering mechanisms of ABC star terpolymers by integrating dynamic self-consistent field theory and variable cell shape methods†

Xuguang Cao, Liangshun Zhang,* Liquan Wang and Jiaping Lin*

A theoretical approach coupling dynamic self-consistent field (SCF) theory for inhomogeneous polymeric fluids and variable cell shape (VCS) method for automatically adjusting cell shape and size is developed to investigate ordered microstructures and the ordering mechanisms of block copolymer melts. Using this simulation method, we first re-examined the microphase separation of the simplest AB diblock copolymers, and tested the validity and efficiency of the novel method by comparing the results with those obtained from the dynamic SCF theory. An appropriate relaxation parameter of the VCS method effectively accelerates the system towards a stable morphology without distortions or defects. The dynamic SCF/VCS method is then applied to identify the richness morphologies of ABC star terpolymers and explore the ordering mechanisms of star terpolymer melts quenched from homogenous states. A diverse range of ordered microstructures, including two-dimensional tiling patterns, hierarchical structures and ordinary microstructures, are predicted. Three types of ordering mechanisms, namely, one-step, quick-slow and step-wise procedures, are discovered in the disorder-to-order transition of ABC star terpolymers. The procedures of microphase separation in the ABC star terpolymer melts are remarkably affected by the composition of star terpolymers and the strength of interaction parameters.

Received 26th March 2014
Accepted 6th June 2014

DOI: 10.1039/c4sm00658e

www.rsc.org/softmatter

1 Introduction

The semiconductor industry has shown considerable interest in the use of block copolymers as lithographic resist materials, for patterning large area substrates with structures of controlled morphologies and a periodicity of ~10–100 nm.[1–6] To date, the development of block copolymer lithography has focused primarily on AB diblock copolymers. It is now known that only a relatively small set of morphologies including lamellae, cylinders and spheres are created by diblock copolymers.[7,8] The cylindrical or spherical microdomains in diblock copolymers generally form close-packed structures with hexagonal symmetry, limiting their device applications.

Tri-block and multi-block copolymers are attracting tremendous attention in the semiconductor community since they generate nanostructures with particular geometries that are unattainable from diblock copolymers,[9–11] significantly enhancing the capabilities of block copolymer lithography.[12,13] An example is the pattern of ABC star terpolymers, which consist of three dissimilar arms connected at a junction point. A striking feature of microstructures of star terpolymers is that the junction points are forced to be in a one-dimensional line.[14] In particular, the star-shaped terpolymers can self-assemble into Archimedean tiling patterns,[15–19] which are not accessible within the phase diagrams of AB or linear ABC block copolymers. More recently, Ross and co-workers have utilized the 3-miktoarm star terpolymers to realize highly ordered Archimedean tiling patterns with tetragonal symmetry,[20–22] which offer an attractive route for the device fabrication of nanolithography compared to the structures of closed-packed arrays in the AB linear diblock copolymer systems.

The complex morphologies of ABC star-shaped terpolymers have also been examined by theory and simulations.[23–28] For instance, Gemma *et al.* performed Monte Carlo simulations to study the self-assembly structures of star terpolymers.[23] Two-dimensional tiling patterns are formed when the three arms are immiscible and the length of the arms comparable. Zhang *et al.* used static self-consistent field theory of polymeric fluids to investigate the phase behaviors of star terpolymer melts.[26] In their work, the novel tiling patterns of star terpolymers were

Shanghai Key Laboratory of Advanced Polymeric Materials, State Key Laboratory of Bioreactor Engineering, Key Laboratory for Ultrafine Materials of Ministry of Education, School of Materials Science and Engineering, East China University of Science and Technology, Shanghai 200237, China. E-mail: zhangls@ecust.edu.cn; jlin@ecust.edu.cn

† Electronic supplementary information (ESI) available: Influences of relaxation parameter on the microphase separation of asymmetric diblock copolymers; VCS simulations for the case of metastable structures; microphase separation of $ABC_{3.5}$ star terpolymer; determination of incubation time and phase separation rate. See DOI: 10.1039/c4sm00658e

partially reproduced, and the triangular phase diagram of star terpolymers with symmetric interaction parameters was successfully constructed.

Although extensive experimental and theoretical studies have been carried out in order to understand the self-assembly of star terpolymers in ordered microstructures, much less is known about the kinetics of microstructure formation and the transition of ABC copolymers under non-equilibrium conditions.[29–32] In particular, the mechanisms of nanostructure formation of ABC star terpolymers are still subject to speculation since the competition between the chain conformation entropy and repulsive interaction energy becomes more complicated than that in diblock copolymers. In this work, we theoretically investigate the self-assembling mechanisms of ABC star terpolymers after quenching from disordered states by a kinetic method. Understanding the ordering mechanisms will help experiments to develop more efficient techniques to control the long-range ordered patterns in lithography and nanoscale device fabrication.

A promising methodology to explore the dynamic behaviors of ABC star terpolymers is a dynamical extension of self-consistent field (SCF) theory for inhomogeneous polymeric fluids.[33–36] The dynamic SCF theory has been successfully applied to tackle the problems of microstructures of block copolymers,[33] which ordering behaviors of phase separation[35,36] and defect motion of microdomains.[37] More recently, a hybrid method of dynamic SCF theory and lattice Boltzmann method was developed by one of the authors to investigate the effects of hydrodynamic on the microphase separation of block copolymers.[38] However, a drawback of the dynamical extension of SCF theory is that it requires a substantial amount of computational cost in the simulations.

In order to reduce the computational cost, it is often convenient to perform the simulations in cells that contain microstructures with one or two periodicities. A disadvantage is that the simulations must be repeated in cells with different shapes and sizes until the stress-free microstructures are generated for given parameters of the block copolymers. A strategy for reducing the cost of repeated calculations is to adjust the cell shape and size as a part of the simulations to obtain final microstructures without residual stress. Recently, a novel numerical technique called the variable cell shape (VCS) method, which is similar to the Parrinello–Rahman–Ray technique for particle-based simulations,[39,40] has been proposed by Barrat *et al.* to explore the equilibrium morphologies of block copolymers.[41] The method automatically tunes the shape and size of the simulation cell to finally achieve a stress-free configuration. Unfortunately, the evolution behaviors of microstructures in the block copolymers cannot be captured by Barrat's method. This motivated us to propose a novel combination method based on dynamic SCF theory, which offers the ability to explore the kinetic behaviors of block copolymers and evolve the systems towards stress-free equilibrium configurations.

In this contribution, we aim to develop a novel method coupling dynamic SCF theory and VCS methods to understand the equilibrium microstructures and ordering mechanisms of complex copolymers. In the combination approach, the dynamic SCF theory not only captures the ordering behaviors of block copolymer melts, but also obtains the equilibrium microstructures. The VCS method automatically adjusts the cell shape and size to finally reach a stress-free configuration. Subsequently, the novel approach was applied to study two different types of block copolymer melts. As a first case, the microphase separation of AB linear diblock copolymers is investigated, and the validity and efficiency of the combination method are examined. The VCS method helps the systems to escape the metastable configurations. The other case investigated is the microphase separation of ABC star terpolymers. The tiling patterns and hierarchical structures of ABC star terpolymers are identified, and three types of ordering mechanism are discovered in the disorder-to-order transition.

2 Model and method

Here, we provide a brief description of the SCF theory used in the present study with a focus on the special extensions. ABC star-shape terpolymer melts are chosen as a model system and generalization to other block copolymers is straightforward. Specifically, we consider melts of n flexible ABC star-shaped terpolymers with a total chain length N in a cell with a volume V. The lengths of the A, B and C arms are $f_A N$, $f_B N$ and $f_C N$, respectively. The average volume fractions f_A, f_B and f_C satisfy the condition $f_A + f_B + f_C = 1.0$. The statistical Kuhn length a and the bulk density ρ_0 of the segments are assumed to be the same for all three species. Spatial length in the model is expressed in units of the reference gyration radius $R_{g0} = a(N_l/6)^{1/2}$ of an ideal linear block copolymer,[42] where N_l is the chain length of the reference linear copolymer, which is expressed as $N_l = (1 - \min(f_A, f_B, f_C))N$. The geometric ratio $\alpha = N_l/N$ is the chain length ratio of reference linear copolymer to star terpolymer. The Cartesian coordinates of any point $\boldsymbol{r}$ in the cell can be expressed by a cell-scaled position vector $\boldsymbol{x}$ whose components lie in $[0, 1]$, *i.e.*, $\boldsymbol{r} = \boldsymbol{h}\cdot\boldsymbol{x}$, where $\boldsymbol{h}$ is the shape matrix of the cell. Within the framework of mean-field approximation to the Edwards model of polymeric fluids,[43,44] the free energy functional F of the star terpolymer melts in units of thermal energy, $k_B T$, is given by the following equation:

$$\frac{\alpha F[\omega_I, \phi_I, \boldsymbol{h}]}{n k_B T} = -\ln Q[\omega_I, \boldsymbol{h}] + \int \mathrm{d}\boldsymbol{x} \Bigg\{ -\sum_I \omega_I(\boldsymbol{x})\phi_I(\boldsymbol{x}) + \sum_{I\neq J} \frac{1}{2}\chi_{IJ} N_l \phi_I(\boldsymbol{x})\phi_J(\boldsymbol{x}) + \frac{1}{2}\kappa_H \left(\sum_I \phi_I(\boldsymbol{x}) - 1 \right)^2 \Bigg\} \quad (1)$$

where the subscripts I and $J \in \{A, B, C\}$ are the species labels, $\phi_I(\boldsymbol{x})$ is the local density field of the I-type species, and Q is the single-chain partition function in the mean potential fields $\omega_I(\boldsymbol{x})$ produced by the surrounding chains. The interaction between the I and J species is characterized by the Flory–Huggins parameter χ_{IJ}. The term with the coefficient κ_H is the

Helfand quadratic approximation, which is used to restrict the deviation of local density fluctuations from the average value. The local density fields $\phi_I(\boldsymbol{x})$ are obtained by the following equation:

$$\phi_I(\boldsymbol{x}) = \frac{1}{Q}\int_0^{f_I} \mathrm{d}s\ q_I(\boldsymbol{x}, s) q_I^{\dagger}(\boldsymbol{x}, f_I - s) \tag{2}$$

In the expression, the functions $q_I(\boldsymbol{x}, s)$ and $q_I^{\dagger}(\boldsymbol{x}, s)$ are the end-segment distribution functions, representing the probability of finding the s-th segment at the rescaled coordinates $\boldsymbol{x}$. The distribution functions are the solutions of the modified diffusion equations:

$$\frac{\partial q_I(\boldsymbol{x}, s)}{\partial s} = R_{g0}{}^2 \nabla_{\boldsymbol{x}}{}^2 q_I(\boldsymbol{x}, s) - \omega_I(\boldsymbol{x})\ q_I(\boldsymbol{x}, s) \tag{3}$$

$$\frac{\partial q_I^{\dagger}(\boldsymbol{x}, s)}{\partial s} = R_{g0}{}^2 \nabla_{\boldsymbol{x}}{}^2 q_I^{\dagger}(\boldsymbol{x}, s) - \omega_I(\boldsymbol{x}) q_I^{\dagger}(\boldsymbol{x}, s) \tag{4}$$

The initial conditions of the abovementioned equations are $q_I(\boldsymbol{x}, 0) = 1$ and $q_I^{\dagger}(\boldsymbol{x}, 0) = q_J(\boldsymbol{x}, f_J) q_K(\boldsymbol{x}, f_K)$ ($IJK \in$ {[ABC], [BCA], [CAB]}), respectively. The non-orthogonal Laplace operator in the rescaled coordinates is expressed as $\nabla_{\boldsymbol{x}}{}^2 = [\boldsymbol{G}^{-1}]_{\alpha\beta} \dfrac{\partial^2}{\partial x_\alpha \partial x_\beta}$, where the indices α and β denote the components along the coordinate axes, and summation over the repeated index is implicit; moreover, $\boldsymbol{G}$ is a metric tensor constructed from $\boldsymbol{h}$ as $\boldsymbol{G} = \boldsymbol{h}^T\boldsymbol{h}$, and $\boldsymbol{G}^{-1}$ denotes the inverse of $\boldsymbol{G}$.

The dynamic SCF theory of polymeric fluids proposed by Fraaije *et al.* is used to study the microstructure evolution of ABC star terpolymers.[33] The diffusion behaviors of the local density fields of segments are assumed to be driven by the gradients of the chemical potentials. The set of density fields $\phi_I(\boldsymbol{x}, t)$ obey the following diffusion equations in the conserved form:

$$\frac{\partial \phi_I(\boldsymbol{x}, t)}{\partial t} = L_I \nabla_{\boldsymbol{x}}{}^2 \mu_I(\boldsymbol{x}, t) + \eta_I(\boldsymbol{x}, t) \tag{5}$$

where $\mu_I(\boldsymbol{x}, t) = \delta F[\omega_I, \phi_I, \boldsymbol{h}]/\delta\phi_I$ are the intrinsic chemical potentials, and the convection terms from the change of cell shape are ignored in the current model. L_I is the mobility of the I-type segment and is assumed to be constant. In the current kinetic model of complex fluids, the entanglement effects of polymeric fluids are neglected. The terms η_I are the Gaussian thermal noises satisfied the fluctuation–dissipation relations:

$$\langle \eta_I(\boldsymbol{x}, t) \rangle = 0$$

$$\langle \eta_I(\boldsymbol{x}, t) \eta_I(\boldsymbol{x}', t') \rangle = -2L_I k_{\mathrm{B}} T \nabla_{\boldsymbol{x}}{}^2 \delta(\boldsymbol{x} - \boldsymbol{x}') \delta(t - t') \tag{6}$$

To obtain the equilibrium states of periodic structures of the ABC star terpolymers, the free energy density of the systems should be minimized with respect to the lattice parameters of the microstructures. For this purpose, the variable cell shape (VCS) method is imposed to evolve the size and shape of cell to approach a local minimum of free energy. There exists a similar particle-based approach, which is the constant pressure molecular dynamic simulations proposed by Parrinello, Rahman and Ray.[39,40] The relaxation of cell obeys the following scheme:[41]

$$\frac{\mathrm{d}\boldsymbol{h}}{\mathrm{d}t} = -\lambda \boldsymbol{h} \boldsymbol{D} \boldsymbol{\Sigma} \tag{7}$$

where $\boldsymbol{h}$ is the tensor of cell shape and λ is a relaxation parameter used to tune the amplitude of cell change. In order to keep a constant volume, a projection operator $\boldsymbol{D}$ on an arbitrary tensor $\boldsymbol{M}$ is introduced, *i.e.*, $\boldsymbol{DM} = \boldsymbol{M} - \dfrac{\boldsymbol{I}}{3}\mathrm{Tr}\boldsymbol{M}$. The tensor $\boldsymbol{\Sigma}$ represents the internal stress tensor produced by polymeric fluids. The components $\Sigma_{\alpha\beta}$ can be calculated by integration of the end-segment distribution functions:

$$\begin{aligned}\boldsymbol{\Sigma}_{\alpha\beta} &= \frac{n}{V}\frac{\partial F}{\partial h_{\alpha\beta}} \\ &= \frac{2nR_{g0}\alpha}{V} G_{\alpha\gamma}{}^{-1} G_{\beta\delta}{}^{-1} \times \int \mathrm{d}\boldsymbol{x} \int \mathrm{d}s \sum_{I=\mathrm{A,B,C}} q_I(\boldsymbol{x}, s) \frac{\partial^2 q_I^{\dagger}(\boldsymbol{x}, f_I - s)}{\partial \boldsymbol{x}_\gamma \partial \boldsymbol{x}_\delta}\end{aligned} \tag{8}$$

In the numerical implementation, the above equations are calculated in the non-orthogonal coordinates. The Laplace operator $\nabla_{\boldsymbol{x}}{}^2$ and the derivative $\nabla_{\boldsymbol{x}}$ with respect to the rescaled spatial coordinates are obtained by using double Fourier transformations between the real and reciprocal spaces. To solve the modified diffusion equations, *i.e.*, eqn (3) and (4), the operator splitting formula introduced by Rasmussen *et al.* is employed.[45] The evolution equation (eqn (5)) of local density fields is implemented by the implicit Crank–Nicholson algorithm.[33] The relaxation equation (eqn (7)) of the cell is integrated by the simple Euler scheme. The thermal noise terms η_I are discretized by an algorithm introduced by van Vlimmeren and Fraaije.[46] In each time step, the self-consistent determination of the potential fields $\omega_I(\boldsymbol{x})$ from eqn (2)–(4) is performed by the Fletcher–Reeves non-linear conjugate gradient method.[47] The iteration is regarded as convergence when a relative deviation of the density fields at each time step becomes less than the error level of 0.01.

All the simulations are implemented in the two-dimensional cell with period boundary conditions. The simulations start from homogenous states, and shallowly quench into ordered states. The VCS method automatically tuning the cell size and shape is used to relax the free energy of system in the evolution of density fields. In the initial states, the spatial mesh is a simple square mesh in two dimensions. After the occurrence of phase separation of polymeric fluids, the shape and size of cells with a fixed volume are changed due to internal stress. This indicates that the spatial resolution for solving the set of equations is not fixed (at a constant mesh size). In our numerical implementations, the solutions of the partial differential equations for the dynamic SCF theory are obtained by considering such a deformation of the mesh. The different mesh sizes will lead to the similar results as long as the spatial resolution of cell is high enough.

3 Results and discussion

3.1 Dynamics of microphase separation in linear AB diblock copolymer melts

We used the AB diblock copolymers to test the validity and efficiency of the combination SCF/VCS method by comparing the results with those of the dynamic SCF theory only. The combined interaction parameter is set as $\chi_{AB}N = 16.0$, and the average volume fraction of the A-type segment has the value of $f_A = 0.5$. The initial configurations of the simulations are the homogenous states, and the initial shape of simulation cells is a square with side length $9.0R_{g0}$. In order to compare the results of the simulations with the VCS method, we also performed reference simulations with the fixed cell shape (FCS) method, which is defined by eqn (7) with $\lambda = 0$.

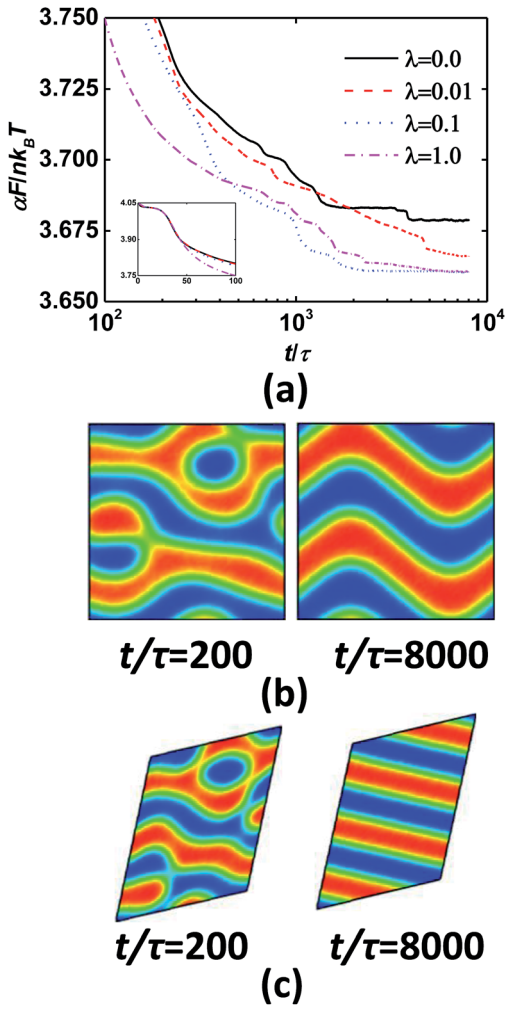

Fig. 1 (a) Temporal evolution of free energy density during microphase separation of symmetric block copolymers after a quenching from homogenous states for various values of the relaxation parameter λ. The reference simulations with $\lambda = 0$ are the case of a fixed cell shape method. The error bars are omitted for the sake of clarity. The inset shows the temporal evolution of free energy density in the initial stage of simulations. (b) Pattern evolution during microphase separation of symmetric block copolymers in a simulation with the fixed cell shape method at times 200τ and 8000τ. τ is the time unit of simulations. (c) Pattern evolution in a simulation with the variable cell shape method at a relaxation parameter $\lambda = 0.1$. The initial states and cell shapes of both simulations are the same. Red and green colors represent A-rich and B-rich regions, respectively.

Fig. 1(a) shows the temporal evolution of the free energy density during the microphase separation of symmetric block copolymers under different relaxation parameters λ. The solid line represents the free energy density of reference simulations with $\lambda = 0.0$, corresponding to the case of FCS method. At the beginning of each simulation, the system is essentially homogenous and the relaxation parameter of cell shape evolution has weak effects on the free energy density (inset of Fig. 1(a)). In the initial stage, a rapid decrease of free energy density indicates the occurrence of phase separation in the block copolymers. Shortly after this stage, the cell relaxation begins to have pronounced effects on the free energy density. The simulations with the FCS method order slowly and trap into a metastable state with higher free energy density, corresponding to case of $\lambda = 0.0$ in Fig. 1(a). In the presence of cell relaxation, the systems order quickly and the free energy densities drop rapidly in a step-wise manner. It should be noted that the free energy densities of systems simulated by the VCS method are lower than that of system simulated by the FCS method.

In order to more directly observe the effects of cell relaxation on the microphase separation of the block copolymers, the morphological snapshots obtained from the FCS and VCS methods in the ordering process are also presented. Fig. 1(b) shows the snapshots of structural evolution for the case of FCS method. The lamellar structure is formed, but the pattern has some defects at time 200τ. Here, τ is the time unit of the simulation. The final pattern of the FCS simulation at time 8000τ is the zigzag structure, which has the features of residual undulation. Fig. 1(c) shows the morphological snapshots of microphase separation simulated by the VCS method. The influence of cell change on the pattern starts to appear after the occurrence of phase separation (time 200τ). Subsequently, the VCS method automatically adjusts the size and shape of the simulation cell to relax the residual stress, and the defects are annihilated by local rearrangement of lamellae. Finally, well-aligned straight lamellar structures are produced in the simulation *via* the VCS method (at time 8000τ).

Inspecting Fig. 1(a) in more detail, one can also check the efficiency of the VCS method by comparing the time dependence of the free energy densities for various values of the relaxation parameter. When the value of relaxation parameter λ is small ($\lambda = 0.01$), it takes a long time to relax the free energy and the system is trapped into a state with a local minimum free energy. For the intermediate value of relaxation parameter λ ($\lambda = 0.1$), the system manages to quickly escape the metastable configurations and reaches a well-aligned lamellar structure, which is illustrated in Fig. 1(c). As the relaxation parameter is large ($\lambda = 1.0$), the free energy density of the system drops rapidly in the initial stage, and then the system is trapped into a metastable state for a long simulation time. The results of the different relaxation parameters suggest that an appropriate value of relaxation parameter effectively accelerates the systems

to overcome free energy barriers and to access the stable microstructures without distortions or defects.

We also examined the asymmetric block copolymer systems and the VCS simulations with initial configurations from metastable structures. The results are presented in the ESI.† As shown in Fig. S1,† the effects of cell relaxation on the temporal evolution of free energy density for the case of asymmetric block copolymers are very similar to those of the symmetric block copolymers, and the VCS method still helps the systems to escape the metastable states. Fig. S2† shows the final configurations of the symmetric and asymmetric block copolymers simulated by the VCS method. The initial configurations of the VCS simulations are chosen from the metastable structures of the FCS method. The results indicate that the VCS method is a convenient way to further lower the free energy of the system.

The observations described above for the case of diblock copolymers demonstrate that the VCS method can automatically adjust the cell size and shape in the evolution of density fields, and an appropriate relaxation parameter effectively accelerates the system towards stable morphologies without distortions or defects. More recently, a similar technique, namely, the system size optimization (SSO) method was proposed by Honda and Kawakatsu to optimize the size of a simulation cell.[48] In their method, the free energy difference is used to determine the change rate of side length of the simulation cell, but the volume of cell is not fixed in the simulations. They found that perfect structures of copolymer melts can be obtained by the SSO method. In our VCS method, the relaxation of cell shape and size is driven by the internal stress and the cell volume is fixed by the action of the projection operator. The well-aligned ordered structures are achieved by our combination method. These facts indicate that the simulation results from the VCS method generally coincide with the findings of the SSO method. This encourages us to apply the novel method to investigate a more complex copolymer system.

3.2 Ordered microstructures and ordering mechanisms in ABC star terpolymer melts

In this subsection, we extended the combination approach of the dynamic SCF theory and VCS methods to investigate the ordered microstructures and ordering mechanisms of microphase separation of ABC star terpolymers. The phase behaviors and ordering behaviors of ABC star terpolymers are very diverse and complicated as they involve many important parameters, such as each arm length and the immiscibility between each pair of species. To reduce the composition parameter space and describe the composition of ABC star terpolymers, we have used the ABC_z nomenclature, in which A and B arms have the same length and the length ratio $N_A : N_B : N_C$ of A, B and C arms has the value of $1 : 1 : z$. The average volume fraction of the C species in the melts is given by $z/(2 + z)$. To further reduce the parameter space of the star terpolymers, we also assume that the C species has the same interactions with the A and B species, *i.e.*, the combined Flory–Huggins interaction parameters $\chi_{AC}N_l = \chi_{BC}N_l$.

In the calculations, the ABC star terpolymers are placed in two-dimensional simulation cells with a volume between $8{R_{g0}}^2$ and $64{R_{g0}}^2$, which is enough to accommodate microstructures with one or two periodicities. A mesh size of 64×64 or 96×96 is used to discretize the cell to ensure the enough spatial resolution for the VCS method. The total chain contour is discretized into 200–500 points, which result from a compromise between the computational demands and resolution. The system is shallowly quenched from an initially homogenous state into an ordered state. Then, the integrated method is applied until the internal stress change of the system at each simulation step reduces to the level of 10^{-3} after the phase separation of polymeric fluids. Multiple realizations with different random numbers are conducted to confirm that the resulting morphologies and ordering behaviors are not accidental. Motivated by our previous findings and to exclude the effects of the relaxation parameter λ on the ordering behaviors of microphase separation, we set the relaxation parameter to $\lambda = 0.1$ to tune the cell size and shape in the simulations of star terpolymers. In this work, we mainly explore how the ordered microstructures and ordering mechanisms of ABC_z star terpolymers are influenced by the compositions and interaction parameters.

3.3 Equilibrium microstructures of star terpolymers

Before investigating the ordering mechanisms of the star terpolymers, the dynamic SCF theory/VCS method is applied to produce two-dimensional equilibrium morphologies. For a comparison with other theoretical studies *via* the Monte Carlo and static SCF methods, we set the symmetric interaction parameters, *i.e.*, $\chi_{AB}N_l = \chi_{AC}N_l = \chi_{BC}N_l$.

Fig. 2(a) shows the ordered microstructures of ABC_z star terpolymers obtained by the dynamic SCF simulations in conjunction with the VCS method at the symmetric interaction parameters $\chi_{AB}N_l = \chi_{AC}N_l = \chi_{BC}N_l = 30.0$. The red, green and blue colors represent A-, B- and C-rich domains, respectively. The observed microstructures are classified into two categories. The first category can be regarded as parallel cylinders with polygonal cross sections, which were characterized as two-dimensional tiling patterns. The tiling patterns were represented by a set of integers [*k.l.m*…], indicating that the *k*-gon, *l*-gon and *m*-gon consecutively meet at each vertex. The polygon-tiling patterns, including [8.8.4], [6.6.6], [8.6.6, 8.6.4] and [10.6.6, 10.6.4], are obtained in the simulations of ABC_z star terpolymers with symmetric interaction parameters. In the [8.8.4] tiling pattern, the two octagonal domains are formed by two different arms and the 4-coordinated domains are composed of the shortest arms. Each vertex is surrounded by two 8-gons and one 4-gon. In the [6.6.6] tiling pattern, three species produce the hexagonal domains and each vertex is surrounded by the three hexagonal polygons. The [8.6.6, 8.6.4] tiling pattern contains two types of vertex in a section, one is surrounded by one 8-gon and two 6-gons and the other is surrounded by 8-gon, 6-gon and 4-gon. Note that the longer arms produce octagonal domains, whereas the shorter arms form two types of domains with different shapes and sizes, *i.e.*, the 4- and 6-coordinated polygons, which alternately surround the 8-coordinated domains. In the [10.6.6, 10.6.4] tiling pattern,

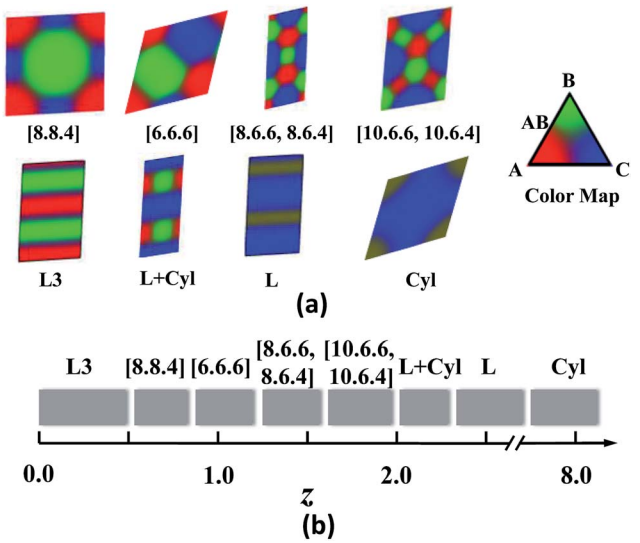

Fig. 2 (a) Representative ordered microstructures for ABC star terpolymers with symmetric interaction parameters. There are four polygon-tiling patterns ([8.8.4], [6.6.6], [8.6.6, 8.6.4] and [10.6.6, 10.6.4]) and four other structures (L3, L + Cyl, L and Cyl). More details about the symbols are stated in the text. In the color map, red, green, and blue denote the A-, B- and C-rich regions of microstructures, respectively. In the L and Cyl structures, the yellow color represents mixing of AB-rich domains. (b) Phase stability regions as a function of length ratio $z = N_C/N_A$. Note that one break is applied to the z axis for the sake of clarity.

there exist three kinds of vertex, one [10.6.6] type and two [10.6.4] types. The longer arms form the 10-coordinated domains encompassed by the six hexagons and four tetragons.

In addition to these polygonal tiling patterns, there also exist additional structures in two dimensions, *i.e.*, three phase lamellae (L3), lamella with alternating cylinders (L + Cyl), lamellae (L) and cylinders (Cyl). In the L3 structure, the layers formed by the shorter arms are sandwiched between the two layers composed of the longer arms. In the L + Cyl structure, the longest arms form the layers and the two shorter arms self-organize into the cylinders with rectangular cross sections. The L and Cyl structures of star terpolymers are similar with the classic lamellar and cylindrical morphologies of linear diblock copolymers, respectively. It should be noted that the microstructures presented here are subject to the two-dimensional restriction and one may not obtain the intrinsic three dimensional morphologies, such as sphere-, gyroid-, and helix-based microstructures.

The one-dimensional phase stability regions of the star terpolymers as a function of the length ratio z are illustrated in Fig. 2(b). When the length ratio z of the C arms to the A arms is small or the C arms are short, since the length of A and B arms is comparable, the system segregates to form A-rich and B-rich lamellae with the minority C component at the interfaces. As the three arms have comparable length, corresponding to the length ratio $0.5 < z < 2.0$, the amount of C arms is sufficient enough to destroy the A and B layers. The star terpolymers tend to self-assemble into the two-dimensional tiling patterns. As the length ratio z increases in the range of $0.5 < z < 2.0$, the various polygonal microstructures including [8.8.4], [6.6.6], [8.6.6, 8.6.4] and [10.6.6, 10.6.4] are successively found. The number of vertices of polygons displays a roughly proportional relationship with the length of C-arms or the volume fraction of the C-species. With an increase in the length ratio z from 0.5 to 2.0, the C-rich polygons undergo the sequence of tetragons → hexagons → octagons → decagons, while the polygons composed of the A or B species vary from octagons, hexagons to the coexistence of hexagons and tetragons.

In the length ratio range of $2.0 < z < 2.5$, in which the volume fraction of A or B species is far smaller than that of the C species, the star terpolymers self-organize into the hierarchical L + Cyl structure instead of the tiling patterns. As the length ratio z further increases to 2.6, since the A and B arms are the minority components, the interaction parameter $\chi_{AB}N_l$ is not enough to ensure the segregation between the A and B species. The domains formed by the mixing A and B species are dispersed in the majority C matrix. In this range of length ratio, the resultant phase behaviors of the ABC star terpolymers are expected to be similar to the behavior of diblock copolymers, and the AB mixed lamellar and cylindrical structures appear in the two-dimensional simulations. Although the A and B arms are much shorter than the C arms, a totally disordered phase eventually emerges.

It is worth pointing out that there exist some experimental and theoretical studies on the richness microstructures of star terpolymers. In the experimental studies, Matsushita and co-workers synthesized a set of ISP star-shaped terpolymers composed of polyisoprene (I), polystyrene (S) and poly(2-vinylpyridine) (P) arms.[14] The tiling patterns (including [6.6.6], [8.4.4], [12.6.4], [8.6.6, 8.6.4] and [10.6.6, 10.6.4]) and hierarchical structures (inducing cylinders-in-lamella, lamellae-in-cylinder and lamellae-in-sphere) are identified by transmission electron microscopy and small-angle X-ray scattering techniques. They also found that the transition sequence of [6.6.6] → [8.8.4] → [12.6.4] → L + Cyl occurs as the P arms (corresponding to the C arms in our model) become longer. More recently, Ross, Manners and co-workers investigated the self-assembly behaviors of a range of ABC star terpolymers with arms of polyisoprene, polystyrene and poly(ferrocenylethylmethylsilane).[20–22] They observed a diverse range of morphologies including cylinders-in-lamella, [8.8.4] and [12.6.4] Archimedean tiling patterns. In our simulations, the complex microstructures observed in the experiments are partially reproduced due to the reduced model of our star terpolymers (Fig. 2(a)). The variation sequence of the pattern transition is [8.8.4] → [6.6.6] → [8.6.6, 8.6.4] → [10.6.6, 10.6.4] → L + Cyl as the volume fraction of C species increases (Fig. 2(b)). Deviations from the experimental observations are sometimes encountered in the theoretical predictions due to unrealistic assumptions made in the model and calculations such as symmetric Flory–Huggins interactions, monodisperse distribution of star copolymers and equal segment size.

Although there is a discrepancy between our theoretical predictions and experimental observations, our results are in general agreement with most of other theoretical results such as Monte Carlo,[23] dissipative particle dynamics,[25] and static SCF

simulations.[26–28] For instance, Zhang *et al.* used the generic spectral method of SCF theory to examine the phase behaviors of star terpolymers.[26] Only the tiling patterns, such as [6.6.6], [8.4.4], [12.6.4], [8.6.6, 8.6.4] and [10.6.6, 10.6.4], are presented in their work, and the corresponding phase diagrams are successfully constructed. As shown in Fig. 2, the equilibrium tiling patterns are reproduced by the dynamic SCF theory in conjunction with the VCS method. The corresponding one-dimensional phase diagram is consistent with the results of Zhang *et al.* In comparison with the Zhang *et al.*'s results, other complex microstructures are also obtained in our work. We also found that the ABC star terpolymers display quite interesting morphology transitions from the tiling patterns to the two length-scale hierarchical structures even in this simplified case of $\chi_{AB}N_l = \chi_{AC}N_l = \chi_{BC}N_l = 30.0$. On the other hand, the static SCF theory used in Zhang *et al.* study deals with the equilibrium structures of polymeric fluids, but does not take into account the kinetics of the microstructures. Note that integrating dynamic SCF/VCS simulations not only provide the equilibrium configurations without internal stress, but also capture the evolution of microstructures of ABC star copolymers.

3.4 Ordering mechanisms of star terpolymers

Next, we focus on the microstructure formation of star terpolymers. To quantitatively measure the segregation behaviors of the three species, the order parameter S_{IJ} is defined to describe the degree of phase separation between the I and J species:[32]

$$S_{IJ}(t) = C_{IJ}\int \mathrm{d}\boldsymbol{x}\left|\phi_I(\boldsymbol{x},t) - \phi_J(\boldsymbol{x},t) - \frac{(f_I - f_J)}{(f_I + f_J + \phi_K(\boldsymbol{x},t))}\right| \quad (9)$$

where the subscripts $IJK \in \{[ABC], [BCA], [ACB]\}$, C_{IJ} is a normalization constant and f_I is the average volume fraction of I species. As the I and J species are miscible, the order parameter S_{IJ} has a value of zero. While the interfaces between the I and J species are sharp, the order parameter S_{IJ} approaches one. Thus, the order parameters S_{IJ} can be used to characterize the degree of phase separation between the I and J species, which is influenced by the composition of star terpolymers and the combined Flory–Huggins interaction parameters.

Fig. 3–5 display three representative order parameter curves observed in the microphase separation of ABC star terpolymers. Fig. 3(a) shows the temporal evolution of order parameters S_{AB}, S_{BC} and S_{AC} for the $ABC_{0.6}$ system quenched to the ordered state at $\chi_{AB}N_l = \chi_{BC}N_l = \chi_{AC}N_l = 30.0$. Fig. 3(b)–(e) show the profiles of the local density fields of star terpolymers at times 50τ, 100τ, 1000τ, and $10\,000\tau$, respectively. After the incubation times marked by τ^i, which is shown in the inset of Fig. 3(a), a sharp increase in the order parameters is observed due to the sudden formation of domains. The slopes K_{BC} and K_{AC} of the order parameter S_{BC} and S_{AC} curves are almost equal, but both are smaller than that of S_{AB} curve. These phenomena indicate that the phase separation between the A and B species is quicker than that of the B and C species or the A and C species. The corresponding density field distributions of A, B and C species at times 50τ and 100τ are shown in Fig. 3(b) and (c), respectively.

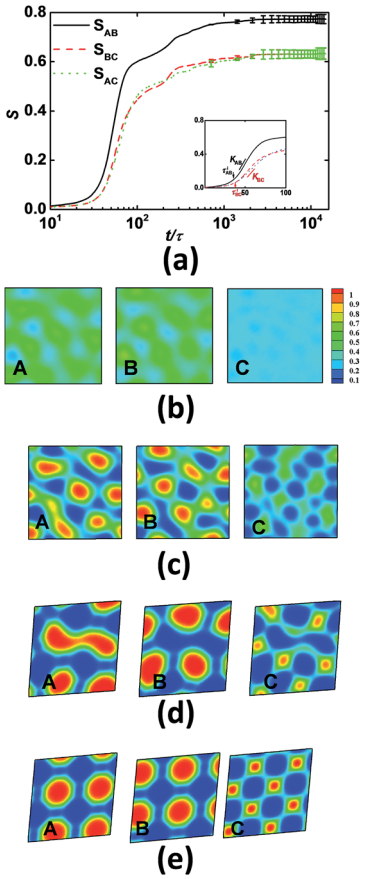

Fig. 3 (a) Temporal evolution of order parameters S_{AB}, S_{BC} and S_{AC} during microphase separation of ABC_z star terpolymers with $z = 0.6$. The melts were quenched from the disordered state at $\chi_{AB}N_l = \chi_{BC}N_l = \chi_{AC}N_l = 0.0$ to the ordered state at $\chi_{AB}N_l = \chi_{BC}N_l = \chi_{AC}N_l = 30.0$. For the sake of clarity, the error bars are only shown in the end stage of the simulations. The inset shows the temporal evolution of order parameters in the time range of $\tau < t < 100\tau$. τ^i_{IJ} and K_{IJ} are the incubation time and rate of phase separation between the I and J species, respectively. Profiles of local density field distributions of the A (left panel), B (middle panel) and C (right panel) species at times 50τ (b), 100τ (c), 1000τ (d) and $10\,000\tau$ (e). Note that all the profiles are displayed in the same color map.

At time 50τ, the intensity difference of density field of each species is weak. At time 100τ, the A and B species form several A-rich and B-rich domains, respectively. The C species is expelled from the A- and B-rich domains and is located at the interfaces between the A and B components due to the junctions of the star terpolymers. In the following stage of the ordering process, the domain size and intensity difference of the density field of each species further increases, which results in a gradual increase of order parameters. Both the A and B species have a tendency to form the octagonal domains, and the C species favors the formation of the tetragonal domains (Fig. 3(d)); however, the pattern is filled with many defects at this stage. The non-perfect transient state further evolves through an extremely slow defect annihilation process. The VCS method plays an important role in reducing the internal stress by changing cell shape and size. Eventually, an ordered [8.8.4]

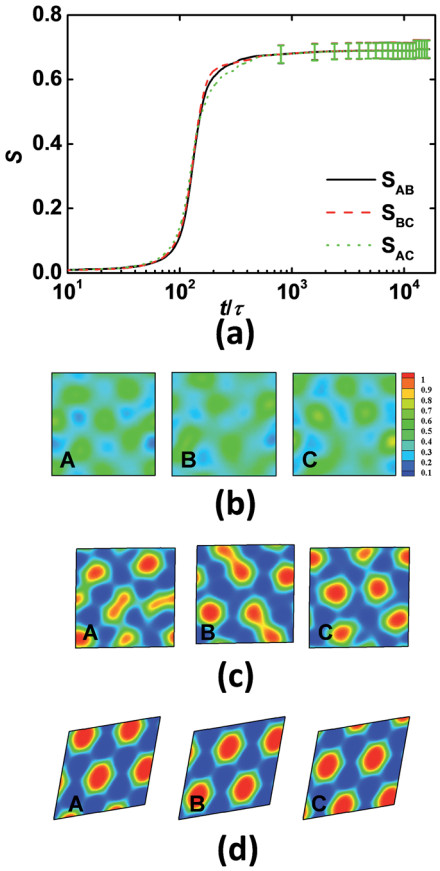

Fig. 4 (a) Temporal evolution of order parameters S_{AB}, S_{BC} and S_{AC} during microphase separation of ABC_z star terpolymers with $z = 1.0$. The melts are quenched from the disordered state at $\chi_{AB}N_l = \chi_{BC}N_l = \chi_{AC}N_l = 0.0$ to the ordered state at $\chi_{AB}N_l = \chi_{BC}N_l = \chi_{AC}N_l = 30.0$. Profiles of local density field distributions of the A (left panel), B (middle panel) and C (right panel) species at times 100τ (b), 220τ (c) and $10\,000\tau$ (d), respectively.

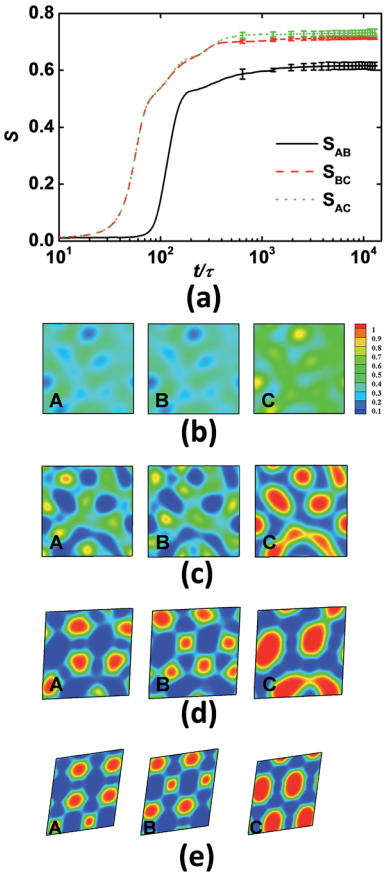

Fig. 5 (a) Temporal evolution of the order parameters S_{AB}, S_{BC} and S_{AC} during microphase separation of ABC_z star terpolymers with $z = 1.5$. The melts are quenched from the disordered state at $\chi_{AB}N_l = \chi_{BC}N_l = \chi_{AC}N_l = 0.0$ to the ordered state at $\chi_{AB}N_l = \chi_{BC}N_l = \chi_{AC}N_l = 30.0$. Profiles of local density field distributions of the A (left panel), B (middle panel) and C (right panel) species at times 50τ (b), 120τ (c), 800τ (d) and $10\,000\tau$ (e).

tiling pattern is formed, which is shown in Fig. 3(e). The A and B arms self-assemble into octagonal domains, and the short C arms self-organize into tetragonal domains.

Fig. 4(a) shows the temporal evolution of the order parameters, *i.e.*, S_{AB}, S_{BC} and S_{AC}, for the $ABC_{1.0}$ system. Fig. 4(b) to (d) show the local density field distributions of A, B and C species at times 100τ, 220τ and $10\,000\tau$, respectively. In the early stage, the emergence of the domains leads to a drastic increase of order parameters. The evolution curves of the three order parameters are almost the same, indicating that the three species simultaneously separate from each other. The corresponding density field distributions of the A, B and C species at times 100τ and 220τ are depicted in Fig. 4(b) and (c), respectively. It is clearly observed that the A, B and C species simultaneously produce the A-, B- and C-rich domains, respectively. The hexagonal microdomains are generated at this stage, but the pattern is filled with many defects. Following the stage of phase separation is also a rather steady evolution of order parameters, and the cell is deformed into a parallelogram. Finally, the three species produce the hexagonal microdomains and each vertex is surrounded by the three hexagonal polygons (Fig. 4(d)).

As the length of the C arms is longer than that of the A or B arms, another type of order parameter curve emerges in Fig. 5. Note that the incubation time of phase separation between the B and C species or the A and C species is about 40τ, but the incubation time of A and B phase separation is about 110τ (Fig. 5(a)). The difference of incubation times is nicely demonstrated by the distribution of local density field of each species at times 50τ and 120τ, which are shown in Fig. 5(b) and (c), respectively. The system initially forms the AB mixed domains in the presence of the majority C component (Fig. 5(b)). As time elapses, the segregation between two minority A and B components occurs (Fig. 5(c)). Moreover, the C-rich domains further coarsen to reduce the surface energy. After the phase separation between the A and B species, the changes of order parameters become slow and the domains further rearrange themselves to form more ordered microstructures. As shown in Fig. 5(d), a complicated ordered microstructure starts to emerge, and the 8-, 6- and 4-coordinated polygons are observed in the pattern at time 800τ. At the end of the simulation, the $ABC_{1.5}$ star terpolymers self-assemble into an ordered [8.6.4, 8.6.6] tiling pattern. The C arms produce the octagonal

domains, and the A and B arms form the tetragonal and hexagonal domains, which alternatively encircle the octagonal domains (Fig. 5(e)). As the length of C arms is further increased, the temporal evolution of order parameters are very similar to that of the diblock copolymers, which is depicted in Fig. S3 of the ESI.†

Thus, three types of order parameter curves in the microphase separation of star terpolymers are observed for the reduced model of star terpolymers and the set of parameters chosen in this study, corresponding to three types of ordering mechanisms of the ABC_z star terpolymers, which are schematically illustrated in Fig. 6. The A-, B- and C-arms are represented by the red, blue and green curves, respectively. The dashed curves denote the interfaces between the different components. As the C-arms are short, the starting times of phase separation are almost the same. The segregation between the longer A and B arms is quick. Moreover, the shorter C arms are randomly distributed at the interfaces, and the shorter C arms slowly rearrange to form domains (Fig. 3). This type of phase separation is named as the quick-slow ordering mechanism designated by M_I, which is shown in Fig. 6(a). When the length of each arm is comparable, three species in the star terpolymer melts are simultaneously segregated from each other (Fig. 4). This is called as the one-step ordering mechanism, which is denoted by M_{II} and is illustrated in Fig. 6(b). Moreover, as the C-arms are long, the phase separation of the star terpolymers has the characteristic of a step-wise ordering mechanism, which is denoted by M_{III} and depicted in Fig. 6(c). One of the three components is segregated from the other two components (1^{st} step), and then the remaining two components are segregated from each other (2^{nd} step). The corresponding order parameter curves are shown in Fig. 5.

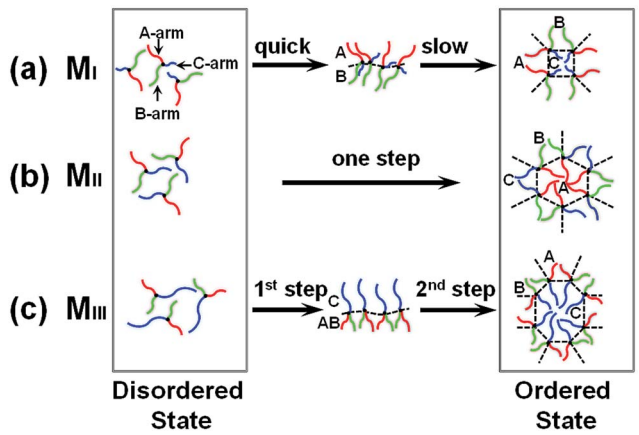

Fig. 6 A schematic illustration of the ordering mechanisms for the disorder-to-order transition of the ABC star terpolymer melts. (a) Ordering mechanism M_I, the two species are quickly separated from each other and the third species was slowly separated from the two species. (b) Ordering mechanism M_{II}, the three species are simultaneously separated. (c) Ordering mechanism M_{III}, the longer arms are firstly separated from the other arms, followed by the segregation of the rest two arms. The red, blue and green curves represent the A-, B- and C-arms, respectively. The black dots represent the junction points of the arms. The dashed curves denote the interfaces of the different species. In the ordered state, the interfaces are simplified by the straight dashed lines.

Experimental investigations of the complicated ordering in triblock copolymer systems were preliminarily undertaken by Hashimoto and co-workers, who examined the microphase separation of polyisoprene-*block*-polystyrene-*block*-poly(vinyl methyl ether) triblock terpolymer (PI-*b*-PS-*b*-PVME).[49] It has been demonstrated that the ordering of such polymer systems proceeds *via* a step-wise mechanism by continuously tuning the temperature or selective solvent content. The 1^{st}-step microphase separation occurs between the PI component and the other two PS and PVME components during the solution casting process, and the 2^{nd} step microphase separation between the PS and PVME components is induced by water. The present study shows that the step-wise procedure of phase separation is simply achieved by quenching the ABC star copolymers from disordered states to ordered states, instead of changing the interaction energy by tuning the temperature or varying the solvent content.

As stated above and shown in Fig. 3–5, the types of order mechanisms are strongly related to the incubation time and rate of phase separation among each species. To systematically examine the ordering mechanisms observed for ABC_z star terpolymers, we further analysed the incubation times and rates of phase separation as a function of the composition of the star terpolymers with different interaction parameters in the initial stage of phase separation. Note that the determinations of incubation times and rates (corresponding to the slopes of order parameter curves) are illustrated in Fig. S4 of the ESI.† Fig. 7(a) shows the incubation times and rates of phase separation as a function of the length ratio $z = N_C/N_A$ for the case of symmetric interaction parameters. Due to the similarity between the S_{AC} and S_{BC} curves, only the incubation times and rates for the B and C species are presented. In the range of length ratio $0.1 < z \leq 1.0$, the incubation times τ^i_{AB} and τ^i_{BC} are almost the same in the phase separation of star terpolymer melts. The incubation time τ^i_{AB} and rate K_{AB} of the A and B species as a function of the length ratio z display a monotonic behavior. However, the incubation time τ^i_{BC} and rate K_{BC} of the B and C species display a non-monotonic behavior. For example, the incubation time τ^i_{BC} reaches a maximum value around $z = 1.0$.

Based on how the incubation times and rates are affected by the length ratio z, the diagram in Fig. 7(a) is divided into three characteristic regimes, which correspond to three types of ordering mechanisms (M_I, M_{II} and M_{III}) in the phase separation of star terpolymers, respectively. In regime I ($0.1 < z < 0.9$), the incubation times of phase separation in the melts are almost equal; however, the rate of phase separation between the A and B species is larger than that of the B and C species. These facts indicate that the starting times of phase separation are almost the same, but the phase separation of A and B species is quicker than that of the B and C species or A and C species. The phase separation of star terpolymers with shorter C-arms corresponds to the ordering mechanism M_I, which is shown in Fig. 6(a). In regime II ($0.9 \leq z \leq 1.3$), the incubation times and rates of phase separation are almost equal, indicating that the three

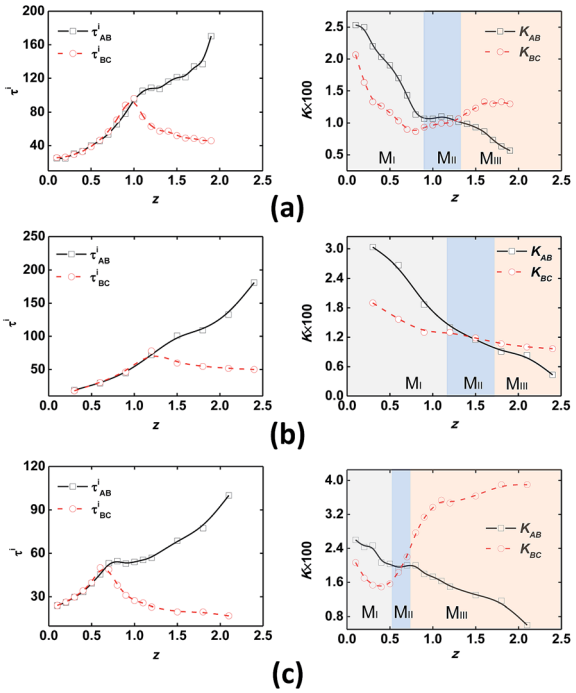

Fig. 7 Incubation times τ^{I}_{IJ} (left panel) and rates K_{IJ} (right panel) of the phase separation between I and J species as a function of length ratio $z = N_C/N_A$ at different interaction parameters: (a) $\chi_{AB}N_l = \chi_{BC}N_l = \chi_{AC}N_l = 30.0$; (b) $\chi_{AB}N_l = 35.0$, $\chi_{BC}N_l = \chi_{AC}N_l = 30.0$; and (c) $\chi_{AB}N_l = 30.0$, $\chi_{BC}N_l = \chi_{AC}N_l = 40.0$. The determinations of incubation times and rates are shown in the Fig. S4 of the ESI.†

species are simultaneously segregated from each other. The phase separation of star terpolymers with comparable arm length satisfies the one-step ordering mechanism M_{II}, which is shown in Fig. 6(b). In regime III ($z > 1.3$), the incubation time of phase separation between the A and B species is longer than that of the B and C species. This phenomenon demonstrates the fact that the C species is firstly separated from the mixed AB domains, followed by the further de-mixing of the A and B species. This type of phase separation corresponds to the step-wise ordering mechanism M_{III}, which is illustrated in Fig. 6(c). This mechanism can be understood as follows: the diblock copolymer melts with low segregation strength necessitate a long incubation time for phase separation to occur.[50,51] In the ABC_z star terpolymer melts, there exists three microphase separations between each pair of species, *e.g.*, A–B pair, B–C pair and A–C pair. The incubation times are determined primarily by the effective interaction parameters $\chi_{IJ}N_{IJ}$, where N_{IJ} is total length of the I and J arms. For the case of ABC_z polymers with $z > 1.3$, $\chi_{AB}N_{AB}$, $\chi_{BC}N_{BC}$ and $\chi_{AC}N_{AC}$ have values of $2\chi_{AB}N_l/(z + 2)$, $\chi_{BC}N_l$ and $\chi_{AC}N_l$, respectively. An increase of C arm length leads to a decrease of the effective interaction parameter $\chi_{AB}N_{AB}$ or a long incubation time of AB phase separation with a slight change of incubation time for the AC or BC phase separation. This results in the two-step ordering mechanism for the ABC_z star terpolymers with symmetric interaction parameters.

In addition, the interaction parameters have effects on the ordering mechanisms of the ABC star terpolymers. Fig. 7(b) and (c) show the data for the incubation times and rates of phase separation for the asymmetric interaction parameters at $\chi_{AB}N_l = 35.0$ and $\chi_{BC}N_l = \chi_{AC}N_l = 40.0$, respectively. The incubation time and rate curves for the asymmetric interaction parameters display similar behaviors for the case of symmetric interaction parameters. The diagrams in Fig. 7(b) and (c) for the star terpolymers with asymmetric interactions are also divided into three characteristic zones. One striking feature of these characteristic zones is that the ordering mechanisms of star terpolymers are dramatically altered by the interaction parameters. To show the effects of interaction parameters, one can choose typical star terpolymers with compositional symmetry, *e.g.*, $ABC_{1.0}$ star terpolymers, as an example. As the interaction parameters are set as $\chi_{AB}N_l = 35.0$ and $\chi_{BC}N_l = \chi_{AC}N_l = 30.0$, the starting times of phase separation are almost equal, but the phase separation rate of A and B species is quicker than that of the other species (Fig. 7(b)). Under these circumstances, the phase separation of the star terpolymers corresponds to the ordering mechanism M_I. In contrast, another scenario is observed for the case of $\chi_{AB}N_l = 30.0$ and $\chi_{BC}N_l = \chi_{AC}N_l = 40.0$, which is shown in Fig. 7(c). Under these settings, the disorder-to-order transition of the star terpolymers obeys the ordering mechanism M_{III} due to the strong immiscibility of the C species with the A or B species.

In the present work, the studies are limited in the ABC_z star terpolymers with symmetric interaction parameters. Three types of ordering mechanisms are found in the reduced model of the ABC star terpolymers. It should be notes that other types of ordering procedure from homogenous states may also take place when the composition of star terpolymers or the interaction parameters among each segment are changed. Taking the previously investigated $ABC_{1.5}$ star terpolymers as an example (Fig. 5 and 6(c)), if the C arms are switched with the B arms and renamed as $AB_{1.5}C$ star terpolymers, the ordering procedure for such star terpolymers may have the following sequence: the B arms are first segregated from the mixed A and C arms, and then the remaining A and B arms are segregated from each other. Correspondingly, the A arms are first separated from the mixed B and C arms for the case of the $A_{1.5}BC$ star terpolymers.

We noted a few limitations of the model used in this study. One limitation is that unrealistic dynamics is introduced into the system by the Parinello–Rahman moves in the variable cell shape method. To avoid the unrealistic dynamics, the simulations should be performed in boxes with fixed cell shape. Nevertheless, stress-free states of phase-separation configurations are not easy to be achieved in the small systems despite the cells having optimized size and shape. In order to rationally explore the dynamics of phase separation of block copolymers, large cell simulations should be conducted to reduce the internal-stress effects on the ordering kinetics. On the other hand, the main reason for integrating dynamic SCF theory and VCS method in our work is that the kinetic pathway of ABC star terpolymers in the reduced model is determined by the free energy landscape of the self-assembling system from the disordered state to ordered states. In small box simulations of dynamic SCF theory without the VCS method, the systems usually trap in intermediate states with residual stress, which leads to high free energy of the systems. Using the combination

approach of the dynamic SCF theory and VCS method, one could yield stress-free intermediate states in the evolution process of the block copolymer melts, which are not easy to obtain in the dynamic SCF simulations.

Another limitation is that the simulations of dynamic SCF theory are performed in the two-dimensional cell. The three-dimensional simulation of dynamic SCF theory with a fixed cell shape method is shown in Fig. 8. The incubation times separate from each other. At time 50τ, the system segregates into the mixed AB domains and C-rich domains. Subsequently, the mixed AB domains form the A-rich and B-rich domains. Finally, the star terpolymers self-assemble into an ordered [8.6.4, 8.6.6] tiling pattern. Such process of phase separation corresponds to the step-wise ordering mechanism of star terpolymers. It should be mentioned that the computational intensity in three dimensions is enlarged greatly due to the recursive calculations of inversion problem of the density fields in the dynamic SCF simulations. Currently, the acceleration techniques *via* graphics-processing-units are addressing the challenges.[52] The SCF simulations can progress up to 60 times faster than those of serial version.

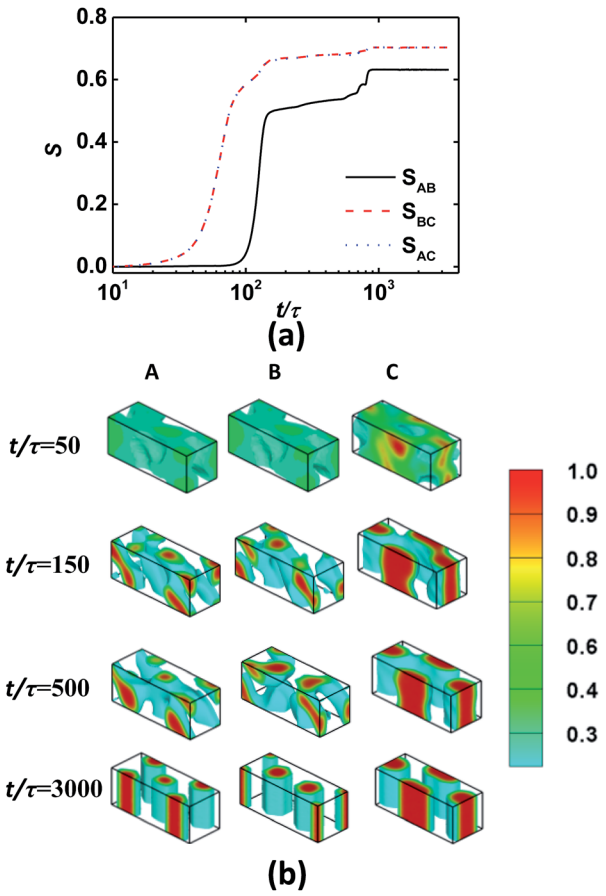

Fig. 8 Microphase separation of the ABC_z star terpolymers with $z = 1.5$ using the dynamic SCF simulations without the Parinello–Rahman moves in the optimization cell. (a) Temporal evolution of order parameters. (b) Profiles of local density field distributions of A (left panel), B (middle panel) and C (right panel) species at times 50τ, 150τ, 500τ and 3000τ.

Despite these limitations, our study may provide valuable guidance to experimentalists on how complex ordered nanostructures of star terpolymers can be tailored in terms of both their thermodynamics and kinetics. For instance, the step-wise microphase separation may be a novel technique to control and create complex morphologies of ABC star terpolymers. For this purpose, one of the three arms must segregate from the other two arms in the first step of ordering, while the remaining two arms are still miscible. The structures exist as a stable state *via* crosslinking of the segregated arms. For the second step, the miscible arms are able to microphase separate in a nanopore or cavity environments formed in the first step. The introduction of geometric frustration to the system in the second step allows the ABC terpolymers to self-assemble into new nanostructures such as helix, toroid and aperiodic structures.[53] The materials with novel morphologies on the nanoscale may have a potential for use in next-generation lithography and photonic crystals,[54,55] which demand a variety of complex nanostructures.

4 Conclusions

To summarize, a combination approach of dynamic SCF theory and VCS methods is developed to probe the ordered microstructures and ordering mechanisms of inhomogeneous polymeric fluids with complex architectures. The disorder-to-order transition of the simplest AB diblock copolymers is studied using this novel combination method. By tuning the cell shape and size in the evolution of the density fields, the copolymer systems are effectively accelerated towards the equilibrium morphologies without distortions or defects. Then, the novel method is applied to explore the complex microstructures and ordering mechanisms of ABC star terpolymer melts. A variety of tiling patterns and hierarchical structures are formed by changing the composition of ABC star terpolymers. As the star copolymer melts are quenched from the disordered states to the ordered states, three types of ordering mechanisms are discovered. When the lengths of two arms are longer than that of the third arm, the two long arms are quickly segregated from each other and the short arm is slowly separated from the formed domains. As the lengths of the three arms are comparable, the three arms are simultaneously segregated from each other. When one of the arms is long, the longer arms are separated from the shorter mixed domains, following the further de-mixing of the shorter arms. In addition, the ordering mechanisms of microphase separation of ABC star terpolymers are strongly affected by the interaction parameters among each segment.

Acknowledgements

This work was supported by the National Natural Science Foundation of China (51203049, 21234002), and the Research Fund for the Doctoral Program of Higher Education of China (20120074120003).

Notes and references

1 M. P. Stoykovich, M. Müller, S. O. Kim, H. H. Solak, E. W. Edwards, J. J. de Pablo and P. F. Nealey, *Science*, 2005, **308**, 1442.
2 I. Bita, J. K. W. Yang, Y. S. Jung, C. A. Ross, E. L. Thomas and K. K. Berggren, *Science*, 2008, **321**, 939.
3 R. Ruiz, H. Kang, F. A. Detcheverry, E. Dobisz, D. S. Kercher, T. R. Albrecht, J. J. de Pablo and P. F. Nealey, *Science*, 2008, **321**, 936.
4 K. G. A. Tavakkoli, K. W. Gotrik, A. F. Hannon, A. Alexander-Katz, C. A. Ross and K. K. Berggren, *Science*, 2012, **336**, 1294.
5 M. Lou and T. H. Epps III, *Macromolecules*, 2013, **46**, 7567.
6 C. M. Bates, M. J. Maher, D. W. Janes, C. J. Ellison and C. G. Willson, *Macromolecules*, 2014, **47**, 2.
7 L. Leibler, *Macromolecules*, 1980, **13**, 1602.
8 M. W. Matsen and M. Schick, *Phys. Rev. Lett.*, 1994, **72**, 2660.
9 V. Abetz and P. F. W. Simon, *Adv. Polym. Sci.*, 2005, **189**, 125.
10 F. S. Bates, M. A. Hillmyer, T. P. Lodge, C. M. Bates, K. T. Delaney and G. H. Fredrickson, *Science*, 2012, **336**, 434.
11 A. J. Meuler, M. A. Hillmyer and F. S. Bates, *Macromolecules*, 2009, **42**, 7221.
12 C. Tang, J. E. Bang, G. Stein, G. H. Fredrickson, C. J. Hawker, E. J. Kramer, M. Sprung and J. Wang, *Macromolecules*, 2008, **41**, 4328.
13 V. P. Chuang, J. Gwyther, R. A. Mickiewicz, I. Manners and C. A. Ross, *Nano Lett.*, 2009, **9**, 4364.
14 Y. Matsushita, *Macromolecules*, 2007, **40**, 771.
15 H. Hückstädt, A. Göpfert and V. Abetz, *Macromol. Chem. Phys.*, 2000, **201**, 296.
16 A. Takano, W. Kawashima, A. Noro, Y. Isono, N. Tanaka, T. Dotera and Y. Matsushita, *J. Polym. Sci., Part B: Polym. Phys.*, 2005, **43**, 2427.
17 K. Hayashida, W. Kawashima, A. Takano, Y. Shinohara, Y. Amemiya, Y. Nozue and Y. Matsushita, *Macromolecules*, 2006, **39**, 4869.
18 K. Hayashida, N. Saito, S. Arai, A. Takano, N. Tanaka and Y. Matsushita, *Macromolecules*, 2007, **40**, 3695.
19 S. Junnila, N. Houbenov, S. Hanski, H. Iatrou, A. Hirao, N. Hadjichristidis and O. Ikkala, *Macromolecules*, 2010, **43**, 9071.
20 K. Aissou, H. K. Choi, A. Nunns, I. Manners and C. A. Ross, *Nano Lett.*, 2013, **13**, 835.
21 A. Nunns, C. A. Ross and I. Manners, *Macromolecules*, 2013, **46**, 2628.
22 K. Aissou, A. Nunns, I. Manners and C. A. Ross, *Small*, 2013, **9**, 4077.
23 T. Gemma, A. Hatano and T. Dotera, *Macromolecules*, 2002, **35**, 3225.
24 X. He, L. Huang, H. Liang and C. Pan, *J. Chem. Phys.*, 2002, **116**, 10508.
25 C.-I. Huang, H.-K. Fang and C.-H. Lin, *Phys. Rev. E: Stat., Nonlinear, Soft Matter Phys.*, 2008, **77**, 031804.
26 G. Zhang, F. Qiu, H. Zhang, Y. Yang and A.-C. Shi, *Macromolecules*, 2010, **43**, 2981.
27 W. Li, Y. Xu, G. Zhang, F. Qiu, Y. Yang and A.-C. Shi, *J. Chem. Phys.*, 2010, **133**, 064904.
28 W. Xu, K. Jiang, P. Zhang and A.-C. Shi, *J. Phys. Chem. B*, 2013, **117**, 5296.
29 K. Fukunaga, T. Hashimoto, H. Elbs and G. Krausch, *Macromolecules*, 2002, **35**, 4406.
30 L. Corté, K. Yamauchi, F. Court, M. Cloître, T. Hashimoto and L. Leibler, *Macromolecules*, 2003, **36**, 7695.
31 S. Ludwig, G. Krausch, R. Magerle, A. V. Zvelindovsky and G. J. A. Sevink, *Macromolecules*, 2005, **38**, 1859.
32 J. Xia, M. Sun, F. Qiu, H. Zhang and Y. Yang, *Macromolecules*, 2005, **38**, 9324.
33 J. G. E. M. Fraaije, B. A. C. van Vlimmeren, N. M. Maurits, M. Postma, O. A. Evers, C. Hoffmann, P. Altevogt and G. Goldbeck-Wood, *J. Chem. Phys.*, 1997, **106**, 4260.
34 C. Yeung and A.-C. Shi, *Macromolecules*, 1999, **32**, 3637.
35 E. Reister, M. Müller and K. Binder, *Phys. Rev. E: Stat., Nonlinear, Soft Matter Phys.*, 2001, **64**, 041804.
36 H. Morita, T. Kawakatsu, M. Doi, D. Yamaguchi, M. Takenaka and T. Hashimoto, *Macromolecules*, 2002, **35**, 7473.
37 L. Tsarkova, A. Horvat, G. Krausch, A. V. Zvelindovsky, G. J. A. Sevink and R. Magerle, *Langmuir*, 2006, **22**, 8089.
38 L. Zhang, A. Sevink and F. Schmid, *Macromolecules*, 2011, **44**, 9434.
39 M. Parrinello and A. Rahman, *J. Appl. Phys.*, 1981, **52**, 7182.
40 J. R. Ray and A. Rahman, *J. Chem. Phys.*, 1984, **80**, 4423.
41 J.-L. Barrat, G. H. Fredrickson and S. W. Sides, *J. Phys. Chem. B*, 2005, **109**, 6694.
42 W. B. Lee, R. Elliott, R. Mezzenga and G. H. Fredrickson, *Macromolecules*, 2009, **42**, 849.
43 S. F. Edwards, *Proc. Phys. Soc., London*, 1965, **85**, 613.
44 G. H. Fredrickson, *The Equilibrium Theory of Inhomogeneous Polymers*, Oxford University Press, Oxford, 2006.
45 G. Tzeremes, K. Ø. Rasmussen, T. Lookman and A. Saxena, *Phys. Rev. E: Stat., Nonlinear, Soft Matter Phys.*, 2002, **65**, 041806.
46 B. A. C. van Vlimmeren and J. G. E. M. Fraaije, *Comput. Phys. Commun.*, 1996, **99**, 21.
47 W. H. Press, S. Teukolsky, W. Vetterling and B. P. Flannery, *Numerical Recipes in Fortran: the art of scientific computing*, Cornell University Press, Cambridge, 1992.
48 T. Honda and T. Kawakatsu, *Macromolecules*, 2006, **39**, 2340.
49 K. Yamauchi, H. Hasegawa, T. Hashimoto, N. Köhler and K. Knoll, *Polymer*, 2002, **43**, 3563.
50 S. R. Ren and I. W. Hamley, *Macromolecules*, 2001, **34**, 116.
51 X. He and F. Schmid, *Macromolecules*, 2006, **39**, 2654.
52 K. T. Delaney and G. H. Fredrickson, *Comput. Phys. Commun.*, 2013, **184**, 2102.
53 A.-C. Shi and B. Li, *Soft Matter*, 2013, **9**, 1398.
54 A. del Campo and E. Arzt, *Chem. Rev.*, 2008, **108**, 911.
55 H. K. Choi, A. Nunns, X. Y. Sun, I. Manners and C. A. Ross, *Adv. Mater.*, 2014, **26**, 2474.